

SINGULAR INTEGRAL EQUATIONS' METHODS FOR THE ANALYSIS OF MICROWAVE STRUCTURES

LIUDMILA NICKELSON AND VICTOR SHUGUROV

VSP

LEIDEN • BOSTON

0175.5
N632

Singular Integral Equations' Methods for the Analysis of Microwave Structures



Liudmila Nickelson and Victor Shugurov

Edited by L.V. Nickelson and T.E. Nickelson



E200600897

///VSP///

Leiden • Boston, 2005

VSP
an imprint of Brill Academic Publishers
P.O. Box 9000
2300 PA Leiden
The Netherlands

Tel: +31 71 535 3500
Fax: +31 71 531 7532
vsppub@brill.nl
www.brill.nl
www.vspub.com

© Copyright 2005 by Koninklijke Brill NV, Leiden, The Netherlands.
Koninklijke Brill NV incorporates the imprints Brill Academic Publishers, Martinus Nijhoff Publishers and VSP.

First published in 2005

ISBN 90-6764-410-2

All rights reserved. No part of this publication may be reproduced, stored in a retrieval system, or transmitted in any form or by any means, electronic, mechanical, photocopying, recording or otherwise, without the prior permission of the copyright owner.

A C.I.P. record for this book is available from the Library of Congress

Printed in The Netherlands by Ridderprint bv, Ridderkerk.

Singular Integral Equations' Methods for the Analysis of Microwave Structures

INTRODUCTION

This book, the result of more than 30 years of research, presents the accumulation of our methods in solving electrodynamical problems. In solving these problems we have developed unique methods based on the theory of Singular Integral Equations (SIE) as well as related computer programs, which we used for numerical analysis.

The subject matter of this book describes the chronological sequence of solving boundary problems and the numerical investigation of proposed microwave structures. Particularly concerned here are those developments in passive devices, such as those controllable through magnetic or electric fields as well as electromagnetic energy transmission lines.

In the early 1970's theoreticians concentrated their efforts on calculations of microstrip lines (MSLs) on infinite dielectric lossless substrates with infinitely thin metal strip conductors of the TEM-approximation (Transverse Electromagnetic). In the past, solutions of these MSL calculations were limited to one-dimensional (1D) or two-dimensional (2D) problems, meaning that most problems could only be solved analytically using conformal mapping. Currently, however, new computer resources designed specifically for complex three-dimensional (3D) electrodynamical problems are able to analyze complex problems such as the electromagnetic field distribution in the human body.

This book will provide many solutions to solving electrodynamical problems. Beginning with calculating simple striplines by a conformal mapping method in chapter two and ending with our numerically investigating electrodynamical characteristics of a heart model that was under microwave radiation. Our SIE methods created would allow anyone to determine the electrodynamical characteristics of certain 2D or 3D-structures.

To see how one might solve an electrodynamical problem using the SIE methods we would start with differential equations having a certain "point source". Then the fundamental solution to the differential equations is used in the integral presentation of an electromagnetic field for each electrodynamical problem that must be solved. This integral presentation would automatically satisfy the differential equations and the density functions would be determined from the boundary conditions.

The solutions of differential equations, obtained by the SIE method were electrodynamically rigorous, as they satisfied the differential equations and the proper boundary conditions. The edge conditions were satisfied due to the inte-

gral presentation of the solution. The practical applications of the SIE methods lead to numerical solutions of the well-determined system of the linear equations that simplified and accelerated the computations. The false roots did not occur applying our SIE methods. The boundary conditions had to be satisfied only on the existing surfaces dividing different materials.

Our SIE methods are universal in that: the cross-section shape can be of any form, the waveguide can be screened or open, the partially homogeneous regions can be dielectric, anisotropic or gyrotropic. These SIE methods are especially effective when the 2D- or 3D-structures have an intricate form and these structures may even include high lossy materials. What we mean by effective is this, we are able to decide very complicated problems with the SIE methods that maybe impossible to solve by other methods.

The SIE methods used to calculate electrodynamical problems enabled us to develop and optimize a number of the microwave devices. Our SIE methods were substantiated through the creation of five devises (patented in the former USSR).

The author's belief is that the SIE methods described in this book will find the widest practical application with experts in the field of microwave techniques in medical, industrial and domestic facilities.

PREFACE

Throughout the book we present examples of using SIE methods in calculating microwave structures. Briefly, in the preface we will present different computation algorithms that were created by our SIE methods. We demonstrate several main formulae for electric and magnetic fields that were used in this book. Expressions of these electric and magnetic fields will be substituted into boundary conditions of certain electrodynamical problems and in this way we will determine the proper solutions. In the following sections we present several SIE methods.

The problems of electrostatics and magnetostatics (chapters 4–7) and the solution of Laplace's equation. In these chapters problems were decided in TEM–approximation. Here the electrostatic field has the integral representation:

$$\dot{E}(z) = - \int_L \frac{\dot{\mu}(t) ds}{t - z} - \sum_{k=1}^m \frac{\dot{A}_k}{z_k - z}, \quad (1)$$

where $z = x_0 + jy_0$ is the coordinate of the point when the boundary conditions are written for an electric field component or when the value of the field component is calculated. Here $t = x + jy$ is the coordinate at the point of contour when the value of the unknown function $\dot{\mu}(t)$ is found. Here $ds = |dt|$ is the contour arc element. The unknown values $\dot{\mu}(t)$ and \dot{A}_k are found after applying the boundary conditions. The value $z_k = x_k + jy_k$ is the coordinate of the point inside of the k -th metal conductor and j is the imaginary unit for the coordinates.

The contours L_ϵ and L_m separate different media in the cross-section of the structure (Fig.1), which are arbitrarily divided into segments. Along these segments the integration is carried out from the lower limit (x_{a_j}, y_{a_j}) to the upper limit (x_{b_j}, y_{b_j}) with an index "j" running from 1 to $n_\epsilon + n_m$. Here n_m is the number of segments of the contours, which is limited to metal. Then n_ϵ is the number of segments of other contours, which is limited to dielectric, semiconductor, ferrite and other materials.

All the contours separating different media are arbitrarily divided into segments and they can be equal or unequal in length. The coordinates of the point "i" (when we formulate the boundary conditions) could be chosen at any place on the segment but the center of the segment is usually the best choice.

Let the structure have in the cross-section several regions bounded by contours L_ε and L_m . Then the boundary conditions have this form:

$$\tilde{\varepsilon}^+ E_n^+(z) \Big|_{L_\varepsilon} = \tilde{\varepsilon}^- E_n^-(z) \Big|_{L_\varepsilon}, \quad (2)$$

where the signs “+” and “-” single out the regions on the left and right side of the contours.

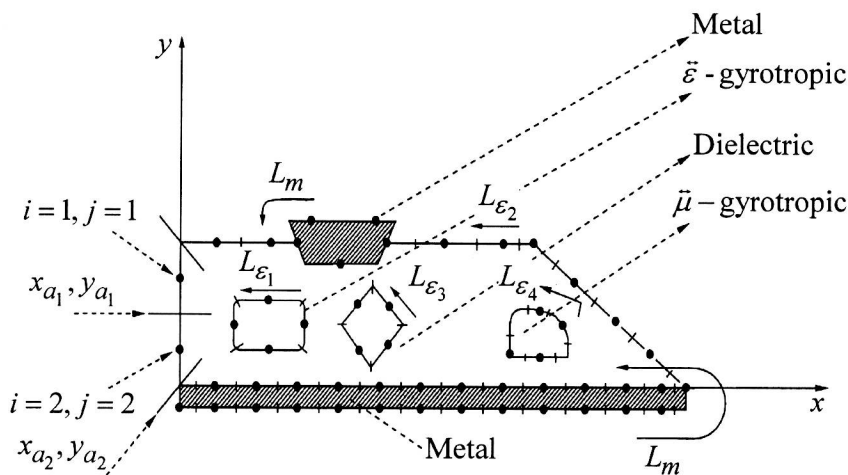


Fig. 1. Cross-section of a strip waveguide line, where L_ε are contours bordering isotropic, anisotropic and gyrotropic media. L_m are contours bordering metal conductors and other designations.

For the contours L_m bordering the perfect metal, the boundary conditions are simpler:

$$E_r^-(z) \Big|_{L_m} = 0. \quad (3)$$

The boundary conditions are formulated for every point “ i ” when “ i ” is running from 1 to $n_\varepsilon + n_m$. Thus the boundary conditions (2) and (3) form the system of linear equations of the order $n_\varepsilon + n_m$. The system is not full because the electric field expression (1) has the unknowns \dot{A}_k and we must add an expression, which gives the values of the potential of each metal conductor (chapter 5). Having the solutions $\dot{\mu}(t_i)$ and \dot{A}_k it is easy to find the electrodynamic characteristics of the MSL (chapters 6–7).

The electrodynamic rigorous solution of Maxwell’s equations to determine the dispersion dependence of the main and higher modes for the regular waveguides, with a cross-section of arbitrary shapes having partial homogeneous materials. We solved Helmholtz’s equation in chapter 8. The

longitudinal components of the electric and magnetic fields are presented in these integral forms:

$$E_z(\vec{r}) = \int_{L_e + L_m} \mu_e(\vec{r}_s) H_0^{(2)}(k_\perp r') ds, \quad (4)$$

$$H_z(\vec{r}) = \int_{L_e + L_m} \mu_h(\vec{r}_s) H_0^{(2)}(k_\perp r') ds, \quad (5)$$

where $E_z(\vec{r})$, $H_z(\vec{r})$ are the longitudinal components of the magnetic and electric fields. Here \vec{r} is the radius vector of the point in the xy plane. Here \vec{r}_s is the radius vector of the contour point (Fig.2). The unknown functions $\mu_h(\vec{r}_s)$ and $\mu_e(\vec{r}_s)$ are determined by the boundary conditions. The $H_0^{(2)}(k_\perp, r')$ is the second kind of Hankel's function of the zeroth order, where $r' = |\vec{r} - \vec{r}_s|$ and $k_\perp = \sqrt{k^2 \varepsilon_r \mu_r - h^2}$ is the transversal wave number.

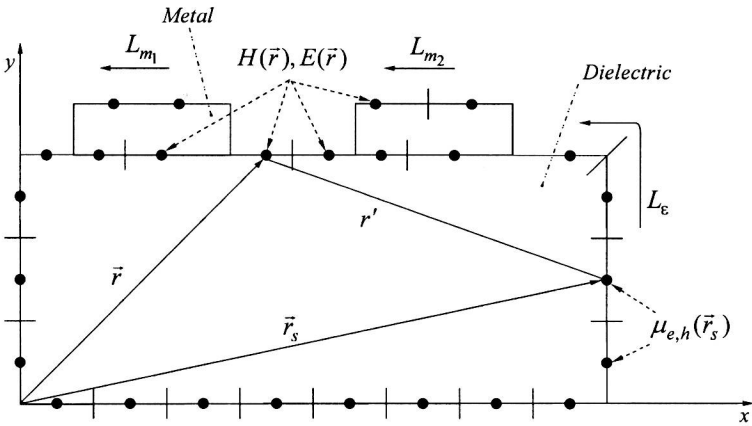


Fig. 2. Cross-section of a slot line, where designations are shown.

From Maxwell's equations, the transversal components H_x , H_y , E_x , E_y of the electromagnetic field can be expressed through two longitudinal components. Substituting the formulae (4) and (5) into the expressions for the field transversal components on the contours bordering isotropic, anisotropic and gyrotropic media:

$$E_\tau^+|_L = E_\tau^-|_L, \quad H_\tau^+|_L = H_\tau^-|_L, \quad (6)$$

on contours bordering metal conductors:

$$E_\tau^+|_L = 0. \quad (7)$$

These terms will contain the Cauchy's type integrals. These integrals become singular at $r' \rightarrow 0$. We applied Sokhotsky-Plemelj formulae to write singular

integrals on the contours. The boundary conditions lead to a system of SIE equations. After applying Bogoliubov–Krylov method we changed the integral equations into the proper system of linear algebraic equations. Setting the system determinant to zero we get certain dispersion equation that permits us to define propagation constants h .

The electrodynamic rigorous solution of Maxwell's equations to determine the dispersion dependence of the main and higher modes for the regular waveguide with an arbitrary shape of the cross-section having partial homogeneous isotropic, anisotropic and gyrotropic materials. The longitudinal components are presented in these forms (chapter 9)

$$\begin{aligned} E_z(\vec{r}) &= \int_L \mu_e(\vec{r}_s) H_0^{(2)}(k_{\perp 2} r') ds + a \int_L \mu_h(\vec{r}_s) H_0^{(2)}(k_{\perp 1} r') ds, \\ H_z(\vec{r}) &= \int_L \mu_h(\vec{r}_s) H_0^{(2)}(k_{\perp 1} r') ds + b \int_L \mu_e(\vec{r}_s) H_0^{(2)}(k_{\perp 2} r') ds. \end{aligned} \quad (8)$$

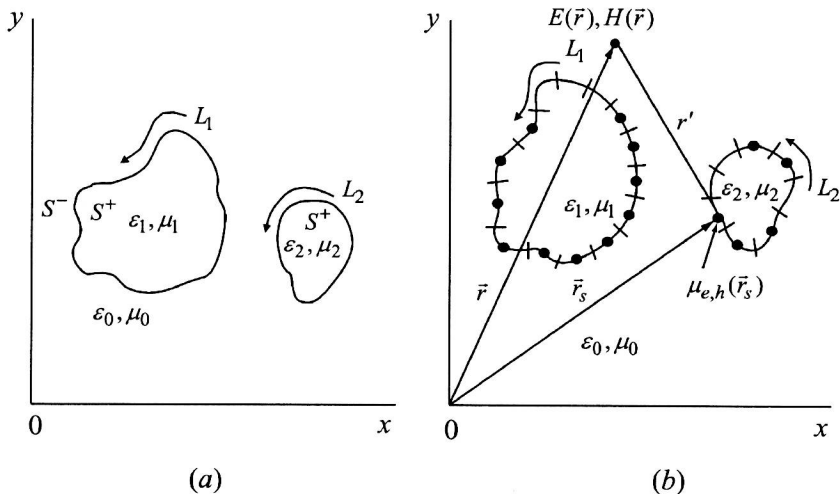


Fig. 3. (a) Cross-section of two coupled $\vec{\epsilon}$ – gyrotropic rods; (b) designations.

The approach to solving electrodynamic problems for regular waveguides with arbitrary shapes (Fig.3) having partly homogeneous isotropic, anisotropic, gyrotropic is the same as was described earlier in the preface. These calculations enable one to develop and optimize a number of the microwave devices. Also to propose new constructions of waveguide transmission lines and different devices on their base.

Solution of Maxwell's equations by the SIE method for open transversally magnetized gyrotropic waveguides (chapter 10). In this chapter, we describe a new method based on the SIE theory. By this, one is enabled to theoretically investigate open waveguides of arbitrary (complex) cross-section geome-

try having transversally magnetized ferrite or semiconductor material. In this chapter the SIE method yields the solution to the problem in the rigorous electrodynamical formulation. This method enables one to analyze the main and higher modes propagating in the investigated waveguide.

The electrodymanical rigorous solution of Maxwell's equations for a 3D isotropic structure of arbitrary form placed in free space (chapter 11). The SIE method was verified when we compared our calculations for 3D isotropic structures with experimental data and with results from science publications. Also in this chapter we solved certain diffraction problems, which enabled us to calculate the back scattering cross-section and other electrodymanical characteristics of different 3D structures (for example Figs.4-6). At the end of this chapter we determined the electrodymanical characteristics of a biological heart model that was under the influence of microwaves. The heart model was illuminated by electromagnetic waves from inside and outside sources.

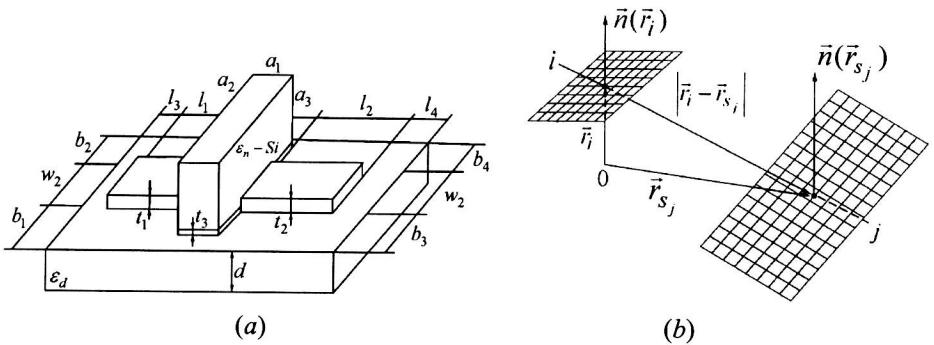


Fig. 4. (a) The configuration of a 3D structure, which is illuminated by outside microwaves; (b) designations.

This 3D structure Fig.4a is a semiconductor sensor and is one kind of dipole probe. It has a sensitive element for detecting a microwave electric field. The sensor is constructed as a symmetric vibrator made of two microstrip conductors with a semiconductor sample of a cuboid form placed between them.

The 3D structure in Fig.5 is a reflector of microwaves containing two-microstrip metallic frames. The ratio of the back reflected signal (toward the microwave source) and the incident microwave field was computed as a function of the frequency.

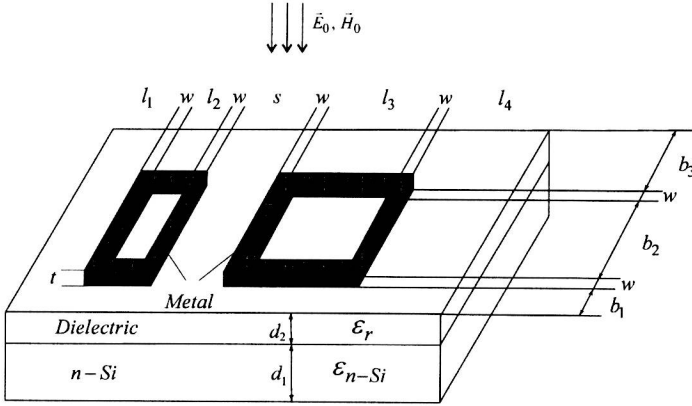


Fig. 5. A structure having a semiconductor–dielectric substrate with two metallic frames placed on it.

A human heart may be under the influence of microwave radiation in the medical examination and therapeutic treatment of patients. When this accrues we can theoretically investigate different electrodynamical characteristics of the heart.

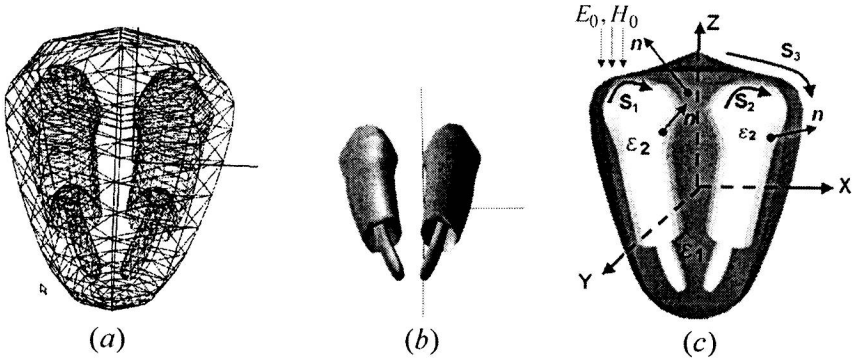


Fig. 6. The model of the heart used in calculations: (a) the surfaces are approximated by triangles, (b) a view of ventricles and atria, (c) certain designations.

An electrodynamical accurate solution of Maxwell’s equations based on the SIE method was used to calculate 3D structures. We investigated 3D heart models when the source of the electromagnetic fields was inside or outside of the heart.

One can determine the components of the electromagnetic field inside and outside of a 3D structure depending on the polarization, wave incidence angle and the electrophysical parameters of the material. In order to calculate the 3D structure and electromagnetic waves interaction it is necessary to solve a diffrac-

tion problem. The known incident electromagnetic wave has components $E_0(\bar{r})$ and $H_0(\bar{r})$, where \bar{r} is the radius vector of a point in which we calculate an electromagnetic field. When solving electrodynamical problems for these 3D structures in Figs.4–6 we wanted to find the scattering or transmitted field. And to present the electromagnetic fields in integral form we used the solutions of Maxwell's equations with electric \vec{j}_e and magnetic \vec{j}_m point sources:

$$\text{rot}\vec{H} = i\omega\varepsilon_0\varepsilon\vec{E} + \vec{j}_e,$$

$$\text{rot}\vec{E} = -i\omega\varepsilon_0\varepsilon\vec{H} - \vec{j}_m.$$

These equations are linear when the general solution is taken as a sum of solutions for an electric wave (when $\vec{j}_e \neq 0$ and $\vec{j}_m = 0$) and as a sum of solutions for a magnetic wave (when $\vec{j}_e = 0$ and $\vec{j}_m \neq 0$).

For the electric $\vec{E}(\bar{r})$ and magnetic $\vec{H}(\bar{r})$ fields the following expressions were derived:

$$\begin{aligned} \vec{E}(\bar{r}) = & \int_s \mu_e(\bar{r}_s) \left(\frac{1}{k^2 \varepsilon \mu} \nabla (\vec{n}(\bar{r}_s), \nabla) + \vec{n}(\bar{r}_s) \right) h_0(z) ds - \\ & - iZ_0 \sqrt{\frac{\mu}{\varepsilon}} \int_s \mu_h(\bar{r}_s) [\vec{n}(\bar{r}_s), \hat{r}] h_1(z) ds, \\ \vec{H}(\bar{r}) = & \int_s \mu_h(\bar{r}_s) \left(\frac{1}{k^2 \varepsilon \mu} \nabla (\vec{n}(\bar{r}_s), \nabla) + \vec{n}(\bar{r}_s) \right) h_0(z) ds + \\ & + \frac{i}{Z_0} \sqrt{\frac{\varepsilon}{\mu}} \int_s \mu_e(\bar{r}_s) [\vec{n}(\bar{r}_s), \hat{r}] h_1(z) ds, \end{aligned}$$

where $h_0(z)$ is a spherical Hankel function of the zeroth order, and the second kind $h_1(z) = -\frac{d}{dz} h_0(z)$ and $z = k\sqrt{\varepsilon\mu}|\bar{r} - \bar{r}_s|$. The wave number $k = \omega/c$, where $\omega = 2\pi f$ and $c = 1/\sqrt{\mu_0\varepsilon_0}$ is the velocity of light in a vacuum. The value $Z_0 = \sqrt{\mu_0/\varepsilon_0} \sim 120\pi$. Values $\mu_e(\bar{r}_s)$, $\mu_h(\bar{r}_s)$ are the electric and magnetic source densities in the point \bar{r}_s of the surface. Here $\vec{n}(\bar{r}_s)$ is the unit normal vector to the surface in the same point \bar{r}_s of the surface. Here ds is an infinitesimal patch of area with a direction that is perpendicular to the surface. The expression $\hat{r} = (\bar{r} - \bar{r}_s)/|\bar{r} - \bar{r}_s|$ is a unit vector in the direction from \bar{r}_s to \bar{r} . This symbol ∇ is a vector operator *del*. The $(\vec{n}(\bar{r}_s), \nabla)$ designation is a dot product and $[\vec{n}(\bar{r}_s), \hat{r}]$ designation is a cross product of two vectors. The densities $\mu_e(\bar{r}_s)$, $\mu_h(\bar{r}_s)$ will be found from the boundary conditions for the electric $[\vec{n}(\bar{r}_1), \vec{E}(\bar{r}_1)^+] = [\vec{n}(\bar{r}_1), \vec{E}^i + \vec{E}(\bar{r}_1)^-]$ and magnetic

$[\vec{n}(\vec{r}_1), \vec{H}(\vec{r}_1)^+] = [\vec{n}(\vec{r}_1), \vec{H}^i + \vec{H}(\vec{r}_1)^-]$ fields on the boundary surfaces, where $\vec{r} \rightarrow \vec{r}_1$ (\vec{r}_1 is a radius vector of a point on the boundary surfaces). These SIE methods can be used to analyse the electrodynamical characteristics of different biological organ models and can be applied to 3D object of any shape or size.

We would like to draw the reader's attention to the fact that value $\mu(t_j)$ takes two values for every point "j". The value $\mu(t_j)$ depends on whether the point is nearing the contour from its left or right side (chapters 8-11). For example (Fig.7):

$$E_z^-(\vec{r}_i) = \sum_j \mu^-(r_{sj}) \int_{a_j}^{b_j} H_0^{(2)}(k_{\perp 2} |\vec{r}_i - \vec{r}_{sj}|) ds ,$$

$$E_z^+(\vec{r}_i) = \sum_j \mu^+(r_{sj}) \int_{a_j}^{b_j} H_0^{(2)}(k_{\perp 2} |\vec{r}_i - \vec{r}_{sj}|) ds$$

on the contour which separate media.

But in electrostatic and magnetostatic problems the values of $\mu(t)$ on the right and left contour sides are equal $\mu^+(t) = \mu^-(t)$.

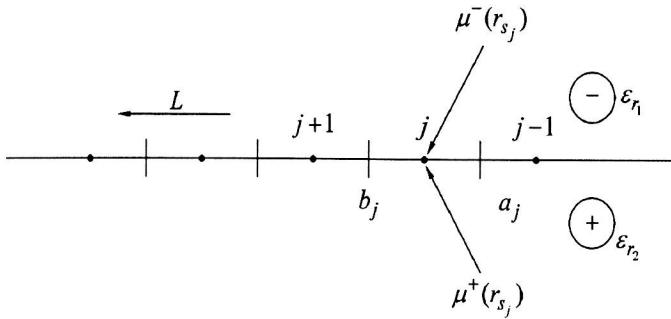


Fig. 7. Designations used in the expressions for the field components.

We have attempted to show some essential points in this preface, which would enable the reader to comprehend our SIE methods and the great diversity in which they can be used. We know that our SIE methods of calculating problems will be extremely helpful in investigating and designing new and unique microwave devices for the future.

Contents

INTRODUCTION	ix
PREFACE	xi
1. CABLE WAVES	1
1.1. Cylindrical waves	1
1.2. The cable wave of coaxial waveguides.....	4
2. THE SIMPLEST STRIPLINES	10
2.1. Presentation of an electric field	10
2.2. The application of conformal mapping	16
2.3. Edge effects of symmetrical striplines.....	18
2.3.1. Short-circuiting metal plane.....	18
2.3.2. The open end.....	20
2.3.3. The flange end.....	22
2.4. Screened lines.....	24
2.4.1. Capacitance of a stripline in a circular cylinder.....	24
2.4.2. Capacitance of a stripline in a rectangular cylinder	26
3. CAUCHY TYPE INTEGRAL AND SOLUTION OF SINGULAR INTEGRAL EQUATIONS	29
3.1. Sokhotsky–Plemelj formulae	29
3.2. Behavior of the Cauchy type integral at the integration contour ends.....	32
3.3. Solution of singular integral equations.....	39
4. ANISOTROPIC MEDIA	41
4.1. The main parameters of ferrite media.....	42
4.2. Magnetic susceptibility tensor taking into account crystallographic anisotropy.....	47
4.3. The permittivity tensor of semiconductor media	54

5. COMMON DEPENDENCIES FOR TRANSMISSION LINES IN TEM - APPROXIMATION	58
5.1. Integral representation	58
5.2. Derivation of singular integral equations	61
5.3. Reciprocity theorem	65
5.4. Connection between matrices of capacitances and inductances	69
5.5. Eigenwaves of a lossless multiconductor transmission line	71
5.6. Eigenwaves of a lossy transmission line	74
5.7. Long line circuits	78
5.8. Realization of the Bogoliubov–Krylov method	81
5.9. Consideration of geometric symmetry	83
6. ANALYSIS OF MICROSTRIP LINES WITH ISOTROPIC AND ANISOTROPIC SUBSTRATES IN TEM-APPROXIMATION BY THE SIE METHOD	86
6.1. Microstrip lines with isotropic substrates	86
6.2. Microstrip lines with n-Si substrates and a comparison of our calculated results with the experimental data	92
6.2.1. Calculated results for MSLs with two-layer n-Si-dielectric substrates	97
6.3. Microstrip lines with GaAs and GaAs–SiO ₂ substrates	100
6.3.1. The calculated results of MSLs with GaAs substrates	101
6.3.2. The calculated results of MSLs with GaAs–SiO ₂ substrates	105
6.4. Microstrip lines with Al ₂ O ₃ –SiO ₂ substrates	111
6.5. Microstrip lines with LiNbO ₃ substrates	117
7. ANALYSIS OF MICROSTRIP LINES WITH GYROTROPIC SUBSTRATES IN TEM-APPROXIMATION BY THE SIE METHOD	133
7.1 Microstrip lines with longitudinally magnetized semiconductor substrates	133
7.1.1. One metal strip MSL	135
7.1.2. Comparison of our calculated results with experimental data	137
7.1.3. Coupled MSLs	138
7.1.4. Losses in geometrically asymmetric MSLs	140
7.2. Meander line on a ferrite substrate	141
7.3. Microstrip lines with transversally magnetized ferrite substrates in the approximation of harmonic functions	150
7.3.1. The differential and integral equations	151
7.3.2. The numerical solution of the integral equations	154
7.4. Microstrip lines with the longitudinally magnetized layer $\vec{\epsilon}$ – gyrotropic substrates	158
7.4.1. A one metal strip MSL with a layer semiconductor–dielectric substrate	158
7.4.2. Comparison of our calculated results with the experimental data	161
7.4.3. The resonance wave attenuation in MSLs on the metal strip thickness and comparison of our calculated results with experimental data	162

7.4.4. Investigation of coupled MSLs with semiconductor–magnetodielectric substrates	166
7.4.5. Coupled MSLs with layer semiconductor substrates	169
7.5. Microstrip lines with longitudinally magnetized substrates having double $(\vec{\epsilon}, \vec{\mu})$ – gyrotropy	172
7.5.1. MSLs with layer semiconductor–ferrite substrates	173
7.5.2. Coupled MSLs with the substrate having double $(\vec{\epsilon}, \vec{\mu})$ – gyrotropy	178
8. SOLUTION OF MAXWELL’S EQUATIONS BY THE SIE METHOD FOR ISOTROPIC WAVEGUIDES	185
8.1. The integral representation for the solution of Maxwell’s equations	185
8.2. Examples of testing the algorithm	191
8.3. Microstrip line dispersion dependences and comparison of our calculated results with data from references	193
8.4. The dispersion dependences of planar slot lines and the comparison of our calculated results with experimental data	196
8.5. The numerical investigation of planar slot lines with asymmetrically placed metal strips and with micron slots between them	200
8.6. The dispersion dependences of the nonplanar slot lines and a comparison of our calculated results with the experimental data	206
8.7. The numerical investigation of nonplanar slot lines with asymmetrically placed strips and micron thicknesses of substrates	209
8.8. The dispersion dependences of dielectric waveguides and the comparison of our calculated results with reference data	212
9. SOLUTION OF MAXWELL’S EQUATIONS BY THE SIE METHOD FOR LONGITUDINALLY MAGNETIZED $\vec{\epsilon}$ – , $\vec{\mu}$ – AND $\vec{\epsilon}$ & $\vec{\mu}$ – GYROTROPIC WAVEGUIDES	216
9.1. The solution for an open circular longitudinally magnetized waveguide	216
9.1.1. Comparison of our calculated results with experimental data	219
9.2. Analysis of longitudinally magnetized $\vec{\epsilon}$ – & $\vec{\mu}$ – gyrotropic waveguides	224
9.3. Some examples of testing our algorithm	236
9.4. Electrodynamical characteristics for $\vec{\mu}$ – gyrotropic slot lines	239
9.5. Electrodynamical characteristics for square–shaped $\vec{\epsilon}$ – gyrotropic waveguides	241
9.6. Electrodynamical characteristics for the $\vec{\epsilon}$ – & $\vec{\mu}$ – gyrotropic one–comb and two–comb waveguides	243
9.7. Electrodynamical characteristics of mirror magnetized ferrite waveguides and comparison of calculated results with experimental data	248